Received: 28 April 2021 | Revised: 29 June 2021 | Accepted: 11 July 2021

DOI: 10.1002/aic.17365

BIOMOLECULAR ENGINEERING, BIOENGINEERING, BIOCHEMICALS, BIOFUELS, AND FOOD

AIChE JOURNAL

Coupling smartphone and CRISPR–Cas12a for digital and multiplexed nucleic acid detection

Tao Yu[1] | Shengwei Zhang[1] | Razvan Matei[2] | William Marx[1] | Chase L. Beisel[1,3,4] | Qingshan Wei[1]

[1]Department of Chemical and Biomolecular Engineering, North Carolina State University, Raleigh, North Carolina, USA

[2]Department of Biological Sciences, Columbia University, New York, New York, USA

[3]Helmholtz Institute for RNA-Based Infection Research (HIRI), Helmholtz Centre for Infection Research (HZI), Würzburg, Germany

[4]Medical Faculty, University of Würzburg, Würzburg, Germany

Correspondence
Qingshan Wei, Department of Chemical and Biomolecular Engineering, North Carolina State University, Raleigh, NC 27695, USA.
Email: qwei3@ncsu.edu

Abstract

Accurate, rapid, and multiplexed nucleic acid detection is of great value for applications in biomedicine and agriculture. Here, we demonstrated a one-step Clustered Regularly Interspaced Short Palindromic Repeats (CRISPR) diagnostic method for the digital and multiplexed detection of both single-stranded (ss) and double-stranded (ds) DNA on a handheld smartphone device. ssDNA targets exhibited faster reaction kinetics of this single-step CRISPR–Cas12a assay than dsDNA counterparts. Under optimized conditions, picomolar levels of ssDNA targets can be detected in 96-well plates by using a benchtop plate reader. The detection sensitivity can be further improved to 5 fM when running the reaction in a microwell-based digital assay chip. Multiplexed detection of hepatitis B virus and human papillomavirus DNA markers was demonstrated on the smartphone-based platform. Finally, the one-step CRISPR–Cas12a assay performed robustly in human serum samples with a recovery rate of ssDNA detection between 96% and 105.6%, suggesting a high potential for clinical diagnostic applications in point-of-care settings.

KEYWORDS
Cas12a, CRISPR diagnostics, digital assay, point-of-care diagnostics, smartphone device

1 | INTRODUCTION

Detection of diseases caused by pathogens at early or asymptomatic stages is of tremendous importance in containing disease spread and improving treatment outcome.[1–6] DNA targets are important biomarkers for many diseases, which can exist in the forms of either single-stranded (ss) or double-stranded (ds) helices. Some pathogens even have hybrid genomes with coexistence of ssDNA and dsDNA sequences. For example, hepatitis B virus (HBV), a partially ds circular DNA virus with a variable-length ssDNA region, can cause severe liver infections, including inflammation, cirrhosis, and even carcinoma, but has no noticeable symptoms during the initial infection stages. Although vaccination has been an effective way to reduce its prevalence, about 3.5% of the global population is infected by chronic HBV.[7] The presence of HBV DNA in serum is a primary biomarker for HBV diagnosis and treatment monitoring, whose concentration can exceed 10^9 copies/ml in serum.[4,5]

Although dsDNA is commonly targeted for medical diagnostics, the promise of ssDNA as detection biomarkers is often overlooked. ssDNA viruses are widespread in different environments, from geothermal springs to human guts.[8] Although many of them (e.g., mycoviruses and ssDNA phages) do not directly infect humans,[9,10] others like adeno-associated virus (AAV), a promising vector for gene therapy,[11] closely impact human health and require frequent bioanalytical examinations to test their presence. In the field of liquid biopsy, cell-free DNA (cfDNA) is an emerging biomarker for noninvasive diagnosis of cancer and other diseases, which contains both ssDNA and dsDNA fragments. Recent studies showed that ssDNA sequencing of cfDNA in human plasma can better deduce nucleosome positioning and the tissues of origin of cfDNA than the

conventional dsDNA-seq methods.[12] Moreover, there is evidence that the ratio of ssDNA to dsDNA could be used as a novel indicator for cancer diagnosis.[13] Finally, viruses with RNA genomes are also very prevalent. Although RNA-specific assays do exit, it is also possible to detect RNA targets with DNA diagnostic assays by converting RNA into ssDNA through a single isothermal step of reverse transcription followed by degradation of the hybridized RNA with RNase H.

Recently, various methods have been developed for the nucleic acid detection, including fluorescent,[14] colorimetric,[15] and electrochemical[16] biosensors. Polymerase chain reaction (PCR) is still considered the standard of care for nucleic acid detection due to its high sensitivity and specificity. However, PCR requires precise thermal cycling and well-trained personnel to operate, making it less than ideal for point-of-care (POC) use. Therefore, development of novel and simpler POC nucleic acid tests that can be applied to both ssDNA and dsDNA targets is still essential to improve the efficiency of medical intervention, especially for the early detection and containment of infectious diseases.

RNA-guided Clustered Regularly Interspaced Short Palindromic Repeats (CRISPR)/Cas systems, including RNA-targeting Cas13a/Cas13b (RNases) and DNA-targeting Cas12a/Cas14 (DNases), have recently been used for highly accurate and rapid nucleic acid detection.[17–22] CRISPR–Cas12a (formerly Cpf1) proteins are RNA-guided enzymes that can recognize and cleave a dsDNA target based on the T nucleotide-rich protospacer-adjacent motif (PAM) through the endonucleolytic RuvC domain. Such genome editing action is well recognized as a self-defense mechanism in the bacterial immune system toward invasive virial species.[23–26] For molecular diagnostic applications, Cas12a-mediated collateral cleavage has been combined with nucleic acid pre-amplification, such as recombinase polymerase amplification (RPA),[26,27] loop-mediated isothermal amplification (LAMP),[28–31] or PCR[23,32] to enable attomolar detection sensitivity. However, the separated pre-amplification and CRISPR reaction processes complicates their use in POC settings.[33] To simplify the assay procedure, efforts to combine CRISPR and preamplification reactions (e.g., RPA) in a one-pot system have been explored. For instance, Wang et al. integrated RPA with Cas12a cleavage into a single reaction tube, where the Cas12a enzyme was stored on the wall of the tube to be physically separated from the RPA mix, and then centrifuged into the reaction mix after the completion of the RPA reaction.[34] This system, named Cas12aVDet, could detect attomolar DNA targets within 30 min. Similarly, Wang et al. stored the Cas12a protein in the tube lid and spun it down after 15 min of RPA preamplification.[35] This one-pot platform, termed OCTOPUS, achieved a limit of detection (LOD) of 1 CFU/ml of foodborne bacteria in less than 50 min total assay time. However, the requirement of a centrifugation step in the above methods for transferring the Cas12a protein to the test solution may hinder their POC applications. In contrast, Yin et al. combined RPA and Cas12a-derived fluorescent detection in a one-pot dynamic aqueous multiphase reaction system, where two reactions occurred simultaneously in spatially separated but connected aqueous phases.[36]

Pre-amplification-free CRISPR assays have also been developed recently. For instance, Dai et al. reported a CRISPR–Cas12a based electrochemical biosensor without using the pre-amplification step, which achieved picomolar sensitivity.[37] Zhang et al. employed a hairpin DNA (hpDNA) linked with methylene blue tag as an electrochemical reporter to improve the interfacial cleavage activity of Cas12a and therefore the detection sensitivity of the electrochemical biosensor. Compared with a conventional liner ssDNA reporter, hpDNA showed lower steric hindrance to Cas12a.[38] Under optimal conditions, this system was able to detect as low as 30 pM target DNA within 60 min. More recently, Nouri et al. reported a label-free electronic sensing platform with a glass nanopore structure to detect HIV-1 DNA biomarkers.[39] In this assay, nanopore analysis was performed after the Cas12a-based CRISPR reaction, the abundance of ssDNA reporter was quantified by nanopore counting, where as low as 10 nM of target DNA was detected within 1 h.

Although electronic biosensors can achieve amplification-free CRISPR detection, they have several drawbacks, such as the complex instrumentation and moderate detection sensitivity. In contrast, the optical detection scheme is more sensitive, specific, and can be easily adapted to POC sensor platforms such as smartphone-based microscopy devices. Recently, handheld and cost-effective smartphone microscopes have demonstrated various POC applications ranging from cancer mutation detection,[40] immunodetection in whole blood,[41] plant disease detection,[42] to environmental monitoring.[43] To our knowledge, the full potential of combining digital CRISPR diagnostics with smartphone devices has not been systematically explored,[44,45] whether for detecting individual or multiple nucleic acids.

Here, we report a one-step Cas12a-based CRISPR diagnostic system running on a smartphone imaging platform (Figure 1). The proposed method does not require any preamplification steps (e.g., RPA, LAMP, etc.) to achieve femtomolar (fM) detection sensitivity by optimizing the assay kinetics and compartmenting the CRISPR reaction in

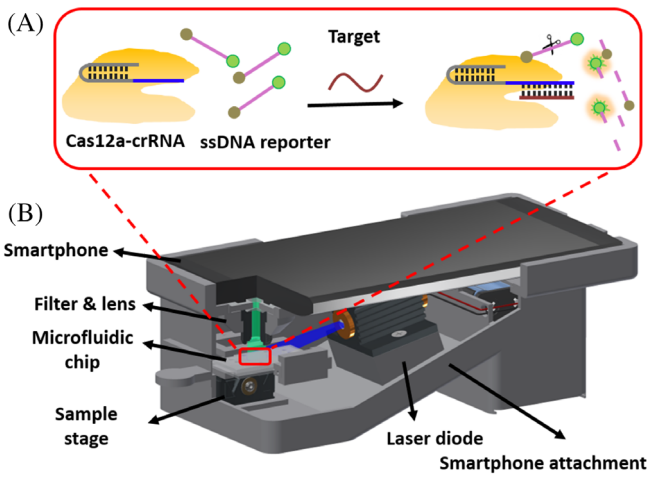

FIGURE 1 Illustrations of the CRISPR assay and smartphone platform for the detection of nucleic acids. (A) Schematic representation of the Cas12a-based detection assay. (B) 3D illustration of the smartphone device with the cutaway view of the attachment [Color figure can be viewed at wileyonlinelibrary.com]

a digital assay format. The assay procedure is different from the conventional CRISPR assay protocols, where the Cas protein and crRNA (and/or target) are preincubated, followed by the addition of reporter molecules (referred to as the two-step reaction).[26,46] In the one-step protocol, the signal is generated and read out in real time after the addition of analytes, and the whole detection procedure can be completed less than 30 min. As a proof of concept, different synthetic DNA sequences including both ssDNA and dsDNA were involved in the assay demonstration. For the solution assay, as low as picomolar (pM) level of DNA was detected under the optimal conditions with a dynamic range of over 4 orders of magnitude for all ssDNA and dsDNA targets by using a benchtop plate reader. For the digital chip assay coupled with smartphone readout, the detection sensitivity can be improved to 5 fM of ssDNA in either standard buffer solutions or serum samples by using a microwell-based digital assay chip. Moreover, multiplexed detection of ssDNA and dsDNA biomarkers related to HBV and human papillomavirus (HPV) was successfully demonstrated on the smartphone.

2 | MATERIALS AND METHODS

2.1 | Chemicals and apparatus

All the chemicals and human serum were obtained from Sigma-Aldrich (MO, USA, analytical grade) and used without further purification and modification. LbaCas12a and NEBuffer™ 2.1 are purchased from New England Biolabs (MA, USA). Microfluidic chips were designed by Adobe Illustrator and fabricated by OAI's exposure system (CA, USA). Polydimethylsiloxane (PDMS) was purchased from Sylgard 184, Dow Corning (MI, USA). Silicon wafers were purchased from Wafer Universe (MA, USA). Ultrapure water (18.3 MΩ cm) was produced by the Milli-Q system (Millipore, Inc., USA) and used throughout the experiments. All of the oligonucleotides used in this work were ordered from Integrated DNA Technologies (Coralville, IA, USA). The sequences of the DNA and microRNA molecules are listed in **Table S1**. Real-time fluorescent data were recorded on a multimode microplate reader (SpectraMax M2, Molecular Devices).

2.2 | Gel electrophoresis analysis

2% agarose gels were prepared using 1× TBE (Tris/Borate/EDTA) buffer (89 mM Tris, 89 mM borate acid, 2 mM EDTA, pH 8.3) and 1× SYBR gel stain. Ten microliters of different reaction products with loading buffer (5:1, v/v) were added to each well. Electrophoresis was run at 100 V for 60 min in 1× TBE buffer at room temperature, and finally the agarose gels were scanned and recorded by using the E-Gel Imager system (Invitrogen, USA).

2.3 | Cas12a/crRNA-based fluorescent assays

All DNA and RNA strands were stored in 10 mM Tris–HCl buffer (pH 7.5) at 10 μM concentrations in a −20°C refrigerator and prewarmed at 37°C for 30 min before mixing. The dsDNA targets were formed by mixing the ssDNA and their complementary sequences (CT1, CT1+PAM, and LCT1+PAM) at the 1:1 ratio in 1× hybridization buffer (20 nM Tris–Cl, pH 7.5, 100 mM KCl, 5 mM $MgCl_2$). For the CRISPR assay, analyte solutions with different concentrations of ssDNA1 were added into the CRISPR reaction reagents, consisting of 40 nM LbaCas12a, 20 nM crRNA, 600 nM F-Q reporter, and 1× reaction buffer (50 mM NaCl, 10 mM Tris–HCl, 10 mM $MgCl_2$, 100 μg/ml BSA, pH = 7.9 at 25°C). The total reaction volume was 80 μl, which was incubated in a microplate reader at 37°C for 45 min with fluorescence measurements (FAM channel, λ_{ex} 490 nm, λ_{em} 520 nm) taken every 30 s.

2.4 | Serum sample denaturation protocol

Briefly, 80 μl of 1× PBS was added into 20 μl of spiked serum sample and the solution was heated to 95°C for 5 min. Then the solution was cooled rapidly to 4°C and kept for 3 min. Then the denatured serum solutions were centrifuged at 14,000 rpm for 30 min at 4°C.

2.5 | Fabrication of microfluidic chips

The microfluidic chips were composed of a layer of silicone elastomer PDMS and a microscope glass slide. UV-curable SU-8 was patterned on the silicon wafer by the standard photolithography protocol as a model to replicate PDMS layers. Holes for fluid control were punched on the PDMS layer after peeling away from the mold. Finally, after the surface plasma oxidization, the PDMS layer and glass slide were spontaneously bonded together. For the digital assay chip, there has three parallel channels, each channel is 3 mm in width and 50 μm in height. Each microwell is about 15 μm in diameter and 20 μm in height, the volume for each microwell is ~3 pl. The fabricated microfluidic chip in the smartphone platform contains five parallel channels with inlets and outlets; each channel is ~300 μm in width and ~100 μm in height.

2.6 | Preparation of a smartphone-based fluorescence reader

The smartphone-based reader consists of an LG V10 smartphone and a 3D-printed optomechanical attachment. The LG V10 smartphone is equipped with a 1/2.6″, 16 megapixels (5312 × 2988) complementary metal-oxide semiconductor (CMOS) image sensor. The built-in smartphone camera lens has a focal length of $f_1 = 28$ mm. The 3D-printed attachment was designed by the Autodesk Inventor software and prepared by 3D printing (uPrint SE Plus, StrataSys). The system included a base attachment to be mounted on the smartphone and a removable sample holder. Inside the attachment, a blue laser diode (465 nm, 100 mW, DTR's Laser Shop) powered by three AAA batteries was connected with a heatsink and was mounted together on the

base attachment. The laser diode was tilted to illuminate the microfluidic chip with an incidence angle of ~15°. The fluorescence signal from the sample was then collected by an M12 lens module ($f_2 = 16$ mm, Uctronics), which gives a magnification that can be calculated as $M = f_1/f_2 \approx 1.75$. A 525-nm band-pass filter (Edmund Optics, #86-354) was placed in front of the smartphone camera as an emission filter to collect fluorescence from the sample as the beam excited the fluorophores. A sample holder was used to hold the microfluidic chip, which could be inserted into the reader during the test. A 1/2″ dovetail translation focusing stage (DT12, Thorlabs) was mounted on the base attachment and was connected to the sample tray to move the sample.

2.7 | Estimation of trans-cleavage rate/activity

Trans-cleavage rate/activity was estimated by calculating the reaction rate V ($V = \Delta F/\Delta T$), where ΔF is the change of fluorescence intensity before reaching the plateau and ΔT is the corresponding reaction time (min).

2.8 | Statistical analysis

Statistical analysis (e.g., box chart) was performed with OriginPro version 8.5. All experiments in this study consisted of three repeats for each sample, unless otherwise indicated. The results are presented as mean ± SD.

3 | RESULTS AND DISCUSSION

3.1 | One-step Cas12a reaction on a smartphone

The principle of the one-step Cas12a/crRNA-based ss(ds)DNA assay is illustrated in Figure 1(A). The crRNA for LbaCas12a consists of two parts: a 21-nt guide sequence (gray region) that can assemble with the Cas12a nuclease and a programmable probe sequence (blue region) that recognizes complementary DNA targets. Fluorophore (FAM)- and quencher (BHQ1)-labeled poly-A (FQ5A) were used as the fluorescent reporter (or ssDNA substrate). The fluorescence background of the detection system is low due to the fluorescence resonance energy transfer (FRET) effect. Upon the addition of target DNA, the crRNA directs Cas12a to assemble target DNA, thereby triggering Cas12a to cleave the FQ5A reporter nonspecifically via the activated RuvC domain. As a result, the fluorescence signal is increased accordingly, which can be quantified by the plate reader or smartphone-based platform.

The smartphone-based fluorescence microscopy attachment was designed and prepared by 3D printing (Figure 1(B)). A bandpass emission filter ($\lambda = 525/15$ nm) and an external lens ($f = 16$ mm) were placed between the smartphone camera and the microfluidic chip. A compact laser diode (465 nm) powered by three AAA batteries was used to illuminate the chip uniformly. The microfluidic chip was inserted into the device by a sample tray, and sat on a moving stage, which was connected to the base attachment via a dovetail translation stage for lateral translocation. The smartphone fluorescent images were captured by the default camera app on the smartphone with an exposure setting of 1 s at an ISO of 150. The captured digital images from the smartphone were analyzed by the ImageJ software on a computer, only the green channels of the RGB images were used for intensity analysis.

3.2 | Kinetics of one-step and two-step Cas12a reactions

To investigate the influence of target structure (sequence length, with/without PAM, ds/ssDNA) and mixing steps on the trans-cleavage activity of Cas12a, we used six DNA targets, including three ssDNA targets: ssDNA1 (20 nt, without PAM), ssDNA1 + PAM (24 nt), and single-stranded long DNA1 (ssLDNA1) + PAM (55 nt), and their dsDNA forms to study the reaction kinetics (see **Table S1** for sequences).

In our one-step reaction protocol, the target was added to the pre-mixed CRISPR reagents in the 1× reaction buffer (including Cas12a, crRNA, and reporters) to initiate the reaction. In contrast, in a conventional two-step reaction, the target was added into the Cas12a/crRNA solution first and incubated for 15 min to activate the Cas12a/crRNA/target complex, and then the fluorescent reporter was added to produce signals (Figure 2).[26] Such a small difference in the sequence of reagent mixing impacts the reaction kinetics, especially for dsDNA targets.

As shown in Figure 2, six different ssDNA and dsDNA targets were tested in the one-step reaction (Figure 2(A–C)) and conventional two-step reaction side by side (Figure 2(D–F)) to investigate the Cas12a DNase activity. Firstly, for the short DNA targets without the PAM sequences (e.g., ssDNA1 and dsDNA1), there were no apparent differences in the reaction kinetics between the one-step and two-step reaction protocols (Figure 2(A,D)). The results confirmed that the activation of the Cas12a from ssDNA does not require a PAM sequence. However, for dsDNA1 without the PAM sequence, there was no obvious trans-cleavage activity of Cas12a observed, in line with many previous studies.[24,26] This was also confirmed by the results of agarose gel electrophoresis **(Figure S1)**, where the ssDNA1 can active Cas12a to cleavage the substrate (95 nt ssDNA), but dsDNA1 cannot. Secondly, for the short DNA targets with the PAM sequences (e.g., ssDNA1+PAM and dsDNA1+PAM), there are no obvious kinetic differences for ssDNA1+PAM between one-step and two-step reactions (black curve, Figure 2(B, E)). However, for dsDNA1 +PAM, the trans-cleavage activity of Cas12a was much higher for the two-step reaction than for the one-step reaction (~2.5 times). This indicates that the pre-incubation step (target+Cas12a/crRNA) played an important role in the reaction process. During the pre-incubation step, Cas12a recognizes the PAM sequence and forms a new duplex structure between crRNA and target strand. The data suggest that the strand separation of dsDNA targets and hybridization to crRNA

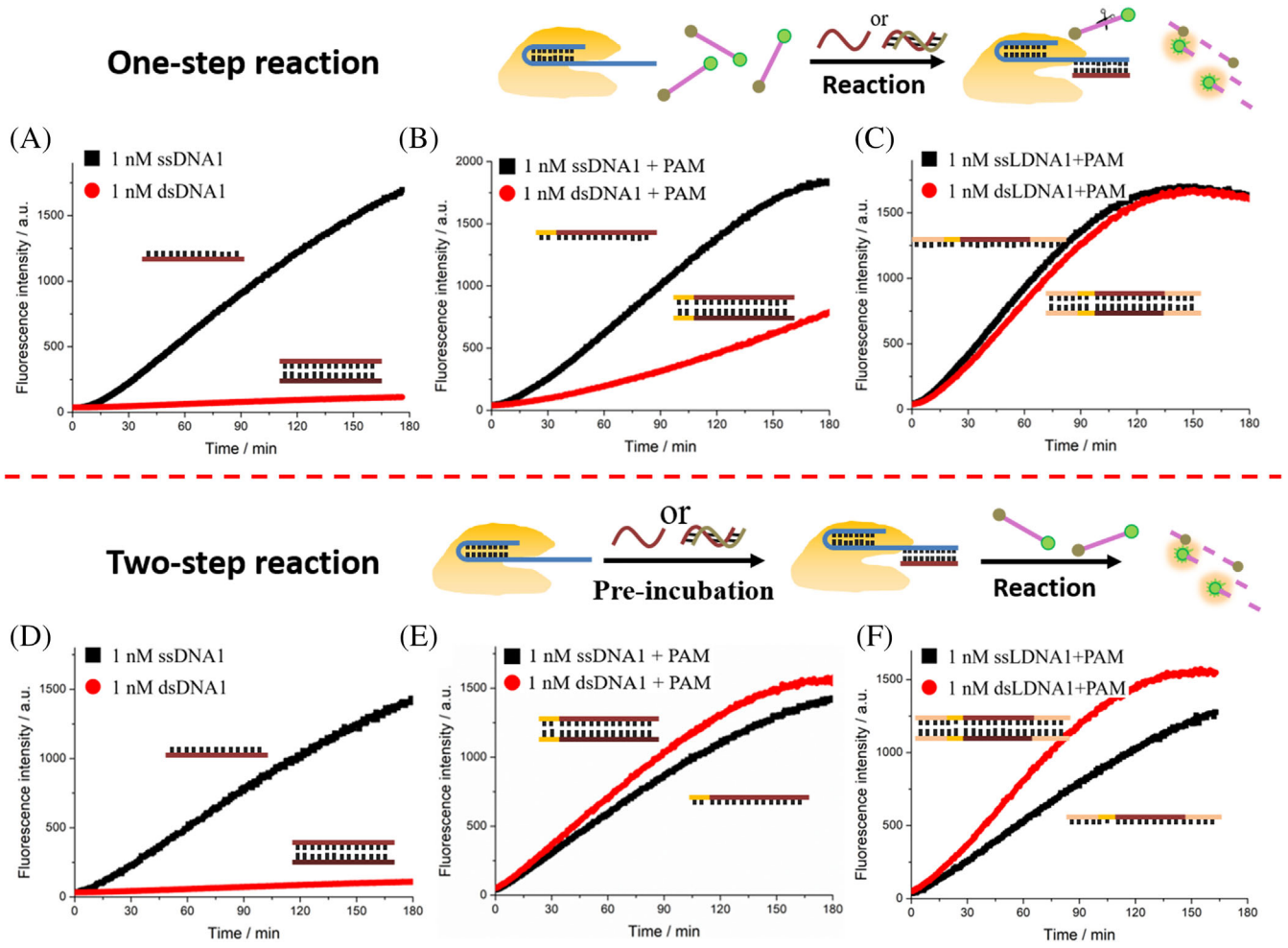

FIGURE 2 Evaluation of the reaction activities of the Cas12a/crRNA system for the one-step (A–C) and two-step reactions (D–F). The concentration of target DNA was set at 1 nM for each reaction, and all the data were collected on the plate reader [Color figure can be viewed at wileyonlinelibrary.com]

(a process referred to as R-loop propagation) is a rate-limiting step for dsDNA detection, as shown in Figure 2(B,E), consistent with previous observation.[47] Finally, for the long DNA targets with PAM sequences (e.g., ssLDNA1+PAM and dsLDNA1+PAM), the activities of the Cas12a were similar for both targets in the one-step reaction (Figure 2(C)). However, for the two-step reaction, ssLDNA1+PAM-activated Cas12a had slightly lower activity than the double-stranded counterpart (Figure 2(F)). These results again suggested that pre-incubation can accelerate dsDNA detection in the reaction. In addition, longer dsDNA targets with sequences on both sides of the PAM could further enhance the trans-cleavage activity of Cas12a system (Figure 2(B,C), red curves). To verify the reliability of the abovementioned conclusions, we changed the crRNA sequence and its corresponding target DNA sequences (ssDNA2 and dsDNA2 with different lengths and with/without PAM) to test the activity of Cas12a, and the results were consistent with DNA1 (**Figure S2**). The results suggest that one-step reaction can greatly simplify the assay process, and only minimally influences the reaction kinetics when compared with the previous two-step method. Kinetically, the one-step method is also more favorable to ssDNA than dsDNA targets.

To better visualize the kinetic differences between ssDNA and dsDNA in the one-step reaction, we expanded the comparison to higher concentration targets (100 nM, **Figure S3**). Without the PAM sequence, the activity of Cas12a initiated by high concentration dsDNA1 was still very low compared with that by ssDNA1 (**Figure S3(A)**). However, in the presence of PAM sequences, although dsDNA1+PAM reacted much slower, it eventually reached the same signal plateau as the ssDNA1+PAM after sufficient reaction time (3 times ssDNA1+PAM, **Figure S3(B)**). This indicates that besides the reaction kinetics, there is essentially no major biochemical difference in the reactions between Cas12a and PAM-appended ssDNA or dsDNA targets. For longer DNA targets with PAM sequences, the time gap between ssDNA and dsDNA to reach the signal plateau was even smaller (~10 min for ss(ds)LDNA1+PAM, **Figure S3(C)**, and ~35 min for ss(ds)DNA1+PAM, **Figure S3(B)**). The results again suggest that the appended sequences on both sides of the PAM would greatly promote the binding of Cas12a and strand separation of the dsDNA, which may be due to the lower binding efficiency of many enzyme molecules to the end of DNA strands.

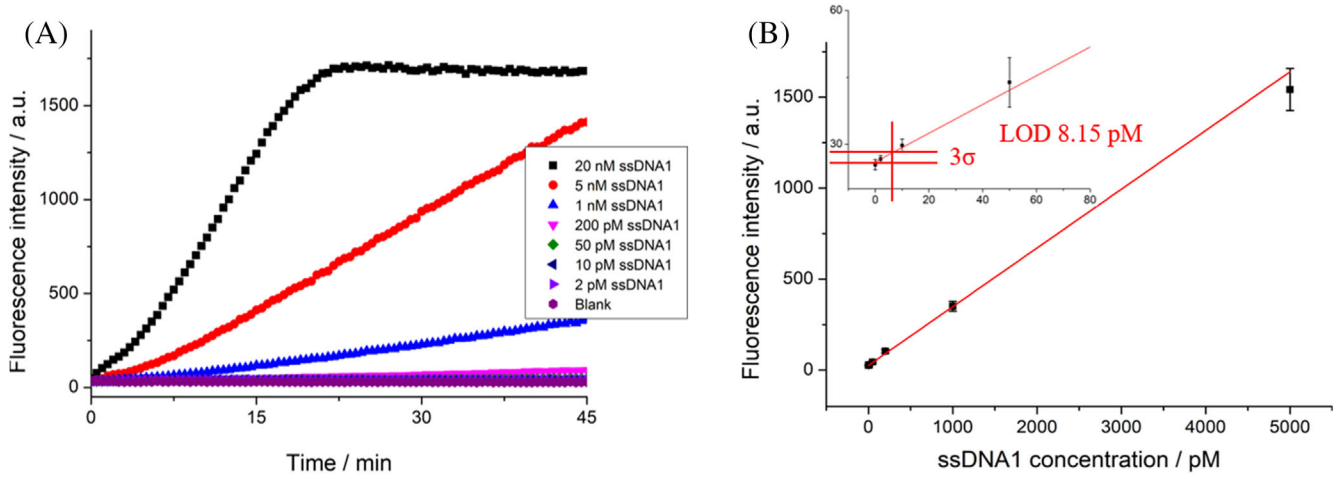

FIGURE 3 LOD quantification for the detection of ssDNA1 in buffer solutions. (A) Plot of fluorescent intensities in the 96-well plate in response to different concentrations of ssDNA1 (from bottom to top: 0, 2 pM, 10 pM, 50 pM, 200 pM, 1 nM, 5 nM, and 20 nM) against with the reaction time. (B) Fluorescent intensity versus different concentrations of ssDNA1 shows a linear relationship ($R^2 = 0.975$) with the ssDNA1 in the range from 0 to 5 nM. Error bars represent the standard deviation of three measurements [Color figure can be viewed at wileyonlinelibrary.com]

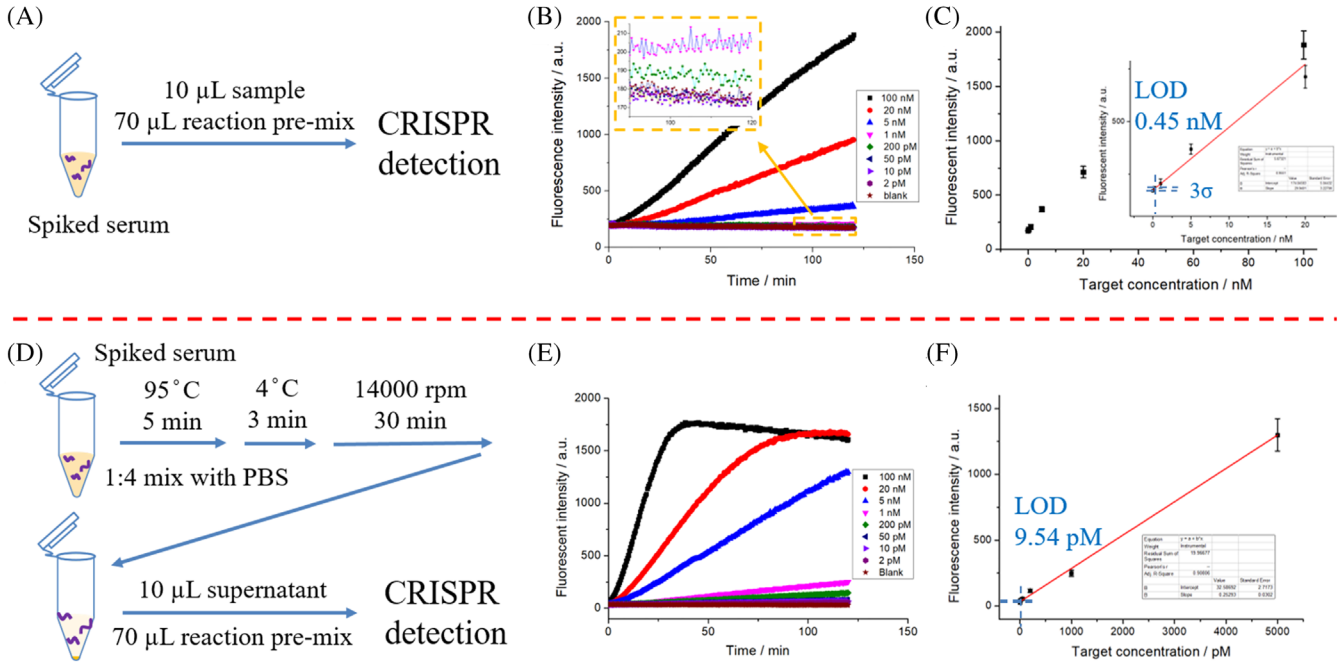

FIGURE 4 Performance of the one-step Cas12a reaction for the detection of ssDNA in (A–C) untreated and (D–F) treated human serum samples. (A,D) Schematic of the treatment procedures of serum samples. (B,E) Time-dependent fluorescent signal measurement by a plate reader. (C,F) LOD quantification for untreated and treated serum samples, respectively. Error bars represent the standard deviation of three measurements [Color figure can be viewed at wileyonlinelibrary.com]

To quantitatively investigate the kinetics of trans-cleavage activity of LbaCas12a, reaction mixtures consisting of 40 nM LbaCas12a, 20 nM crRNA, 0.1 nM ssDNA or dsDNA targets, and different concentrations of FQ5A reporters (0.01, 0.1, 0.2, 0.5, 1, 2, and 5 μM) were prepared for the Michaelis–Menten analysis (**Figure S4**). Reactions were performed at 37°C with fluorescence measured every 30 s. The initial velocity (V_o) was plotted against the substrate concentration to obtain the Michaelis–Menten constants K_m:

$V_o = (V_{max}\ [S])/(K_m + [S])$,where V_{max} is the maximum reaction rate, $[S]$ is the substrate (FQ5A) concentration, and K_m is the Michaelis constant. The turnover number (K_{cat}) was determined by using the equation:

$K_{cat} = V_{max}/E_t$,where E_t is the total activated enzymes (0.1 nM for this reaction, limited by the target concentration). For the two-step reaction, the calculation showed that ssLDNA1+PAM-activated LbaCas12a–crRNA complex had a turnover number (K_{cat}) of ~1.39

and a catalytic efficiency (K_{cat}/K_m) of 2.9 × 10^6 s^{-1} M^{-1}, where the corresponding dsLDNA1+PAM-activated complex had a K_{cat} of ~2.71 and K_{cat}/K_m of 4.8 × 10^6 s^{-1} M^{-1} (**Figure S4(E)**). The results are consistent with the literature reports. Later, the Michaelis–Menten analysis for 12 different assay conditions (one-step and two-step reactions with six different targets, ssDNA1, dsDNA1, ssDNA1+PAM, dsDNA1 +PAM, ssLDNA1+PAM, and dsLDNA1+PAM) was demonstrated. The calculated values of K_{cat}, K_m, and K_{cat}/K_m are listed in **Table S2**, which are consistent with the results of Figure 2, suggesting that ssDNA target in the absence of PAM sequence is approximately 5 times faster than dsDNA counterpart in terms of reaction rate for the one-step protocol.

From the abovementioned experiments, it can be concluded that the Cas12a system is a general method for both ssDNA and dsDNA (with PAM) detection. Cas12a-based diagnostics is also more flexible than conventional PCR by its ability to detect very short DNA targets (e.g., 20 nt), which is equal or even shorter than most PCR primers in length. For dsDNA detection, however, a few conditions need to be met to enable rapid Cas12a-based detection: (1) a PAM sequence is required to be present in the target; (2) longer target sequences are preferred to facilitate Cas12a binding; and (3) a pre-incubation step (as in the conventional two-step reaction) will speed up the recognition of the dsDNA targets, thereby increasing the overall reaction rate for the assay. In contrast, the Cas12a system seems better suited for ssDNA detection, as (1) no PAM sequence is required for the ssDNA targets; (2) the reaction kinetics of the Cas12a assay is minimally influenced by the length of ssDNA target; and (3) the reaction rate is insensitive to the reaction protocol (e.g., one-step vs. two-step reactions).

Moreover, the one-step reaction protocol is more preferred for the POC applications, as it demonstrates the feasibility of premixing of all CRISPR reagents in one pot and reaching a high reaction rate (**Table S2**). In addition, the one-step protocol is advantageous over the two-step reaction in the detection sensitivity, because the Cas12a/crRNA could also potentially collaterally cleave the ssDNA targets during the pre-incubation step, even in the absence of fluorescent reports.

TABLE 1 Recovery rates of the one-step CRISPR–Cas12a assay for ssDNA detection in the treated serum sample (spiked ssDNA in undiluted serum sample)

Added (nM)	Determined (nM)	Recovery	RSD% ($n = 3$)
1	0.986	98.6%	4.3
0.2	0.192	96.0%	4.1
0.05	0.0528	105.6%	5.7

Abbreviations: RSD, relative standard deviation; ssDNA, single-stranded DNA.

3.3 | Optimization of the CRISPR assay for ssDNA detection

In order to achieve the best performance of Cas12a for detecting ssDNA targets, the assay conditions were further optimized by testing the different stoichiometric ratios of the reaction components. To do that, the concentration of Cas12a was set at 40 nM, and the

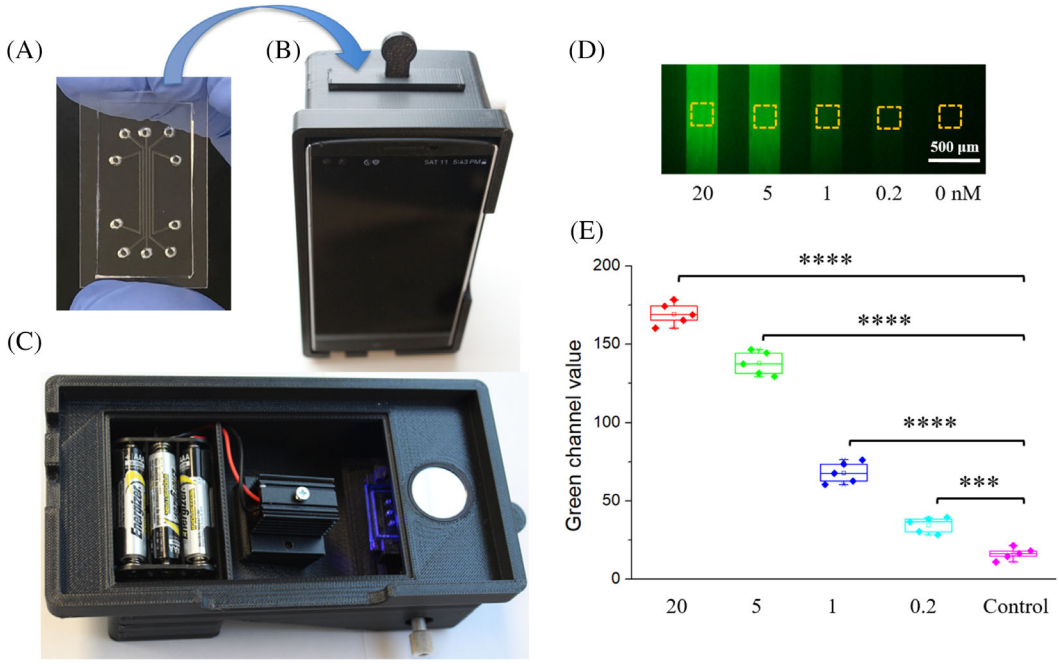

FIGURE 5 The smartphone–CRISPR detection platform. Photographs of (A) the microfluidic chip, (B) smartphone device, and (C) the interior design of the attachment. (D) A representative fluorescence image of microfluidic channels captured by the smartphone. (E) The channel intensities analyzed in a box chart. The experiments were repeated five times for the statistics. ***represents $p < 0.001$, and ****represents $p < 0.0001$ [Color figure can be viewed at wileyonlinelibrary.com]

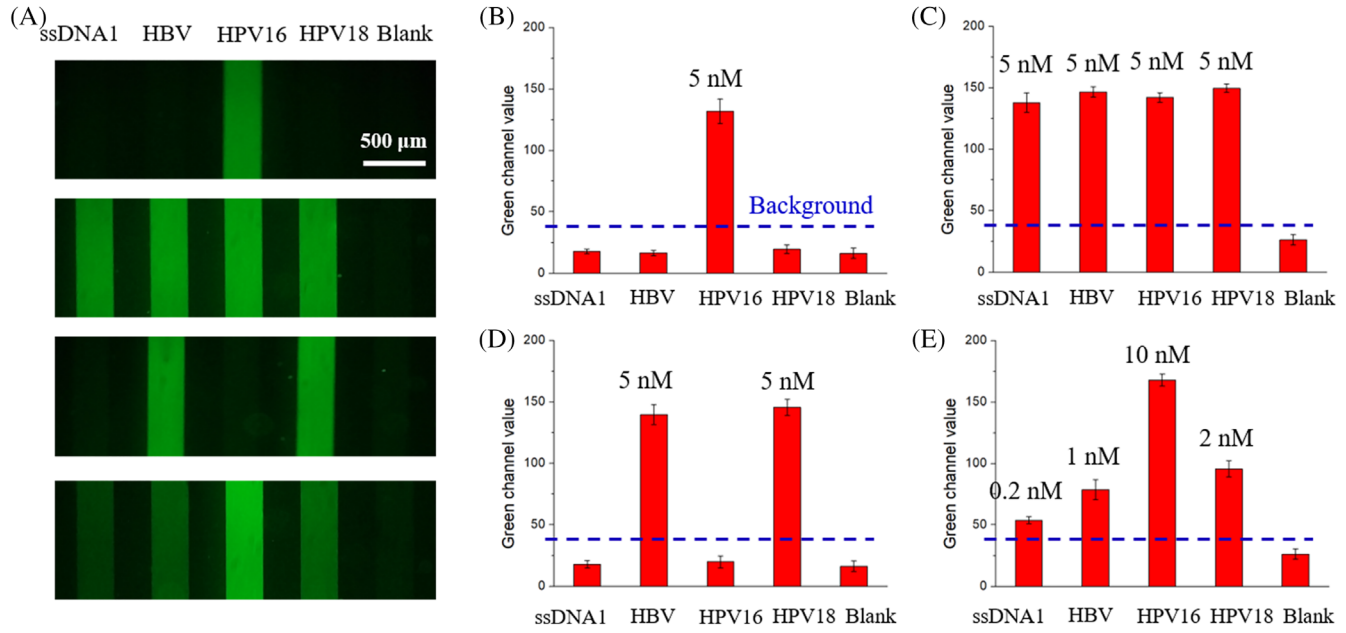

FIGURE 6 Multiplexed detection of ssDNA1, HBV ssDNA, HPV16, and HPV18 dsDNA using the smartphone platform. (A) Smartphone fluorescence images of different testing samples (ISO 250, exposure time 1 s), and (B–E) the corresponding *G* values of each channel for each sample. The actual concentrations of exist targets were labeled on the top of the intensity columns. The blue dashed line represents signals obtained from pure 0.2 nM ssDNA1 target [Color figure can be viewed at wileyonlinelibrary.com]

concentration of crRNA varied from 80, 60, 50, 40, 30 to 20 nM, representing a Cas12a-to-crRNA ratio of 1:1.25 to 1:0.5. ssDNA1 were selected as a target model to optimize the ratios, and its concentration was varied from 50 pM, 200 pM, 5 nM, to 20 nM (**Figure S5**). We found that the combination of 40 nM Cas12a and 20 nM crRNA (Cas12a-to-crRNA 1:0.5) achieved the highest trans-cleavage rate (see Section 2) at all different target concentrations. The results suggest that an excess amount of crRNA (Cas12a-to-crRNA ratio <1) would greatly hinder the reaction kinetics, which is probably caused by the competition between free crRNA and crRNA–Cas12a complex to bind with the targets. After the optimization, the detection sensitivity and dynamic range of the assay were quantified by using a series of dilutions of ssDNA1 (from 0, 2 pM, 10 pM, 50 pM, 200 pM, 1 nM, 5 nM to 20 nM) in standard buffer solutions (1× PBS). At first, this assay was conducted for 120 min, and fluorescent intensities were recorded every 30 s (**Figure S6(A)**). We can find that the signal resolution of low-concentration target (2 pM) increases with the reaction time (**Figure S6(B–F)**), and 2 pM target can be clearly distinguished from the background at 45 min (**Figure S6(D)**). In the following plate reader-based experiments, the fluorescence intensities at the 45-min time point were used for the quantitative analysis (Figure 3). The signal of 20 nM target plateaued at about 20 min into the reaction, and that data were therefore not included in the LOD quantification (Figure 3(A)). By plotting the fluorescence intensity versus the concentration of ssDNA1, an almost linear calibration curve was obtained (Figure 3(B)). The LOD was calculated by finding the corresponding ssDNA1 concentration where its assay signal is above that of the blank (zero) plus 3× the SD of the blank (inset of Figure 3(B)). The LOD was quantified to be 8.15 pM for the one-step assay, which is among the best for Cas12a to detect nucleic acids without any pre-amplification steps.[26,47,48]

Next, the robustness of this assay in complicated biofluid samples such as human serum was investigated. Undiluted healthy human serum samples were spiked with different concentrations of ssDNA1 solutions in a volume ratio of 19:1, and then 10 μl of spiked samples (95% serum) were detected by using the one-step CRISPR assay (Figure 4(A)). As shown in Figure 4(B), the fluorescent background of the serum samples (~180 a.u.) was much higher than the buffer solutions (~ 20 a.u.) (Figure 3(A)). In this situation, an LOD of 450 pM was achieved in 95% human serum (Figure 4(C)), which is 2 orders of magnitude higher than that of buffer solutions (Figure 3(B)). However, if the serum samples were treated by a protein denaturation protocol[49] before adding into the CRISPR reagents, the performance of ssDNA detection could be significantly improved (Figure 4(D)). The test results are shown in Figure 4(E,F), where an LOD of 9.54 pM was achieved, which is close to the performance in the buffer solution (Figure 3(B)). The recovery rates of ssDNA1 detection in the treated human serum samples were higher than 96% for all samples tested ([ssDNA] = 0.05, 0.2, 1 nM) **(**Table **1).**

3.4 | One-step Cas12a assay in microfluidic chips combined with smartphone readout

We then investigated the performance of chip-based CRISPR assay coupled with the smartphone readout. A 3D-printed smartphone fluorescence reader device was prepared as described in the Section 2. Two different microfluidic chips, a linear channel chip and a digital

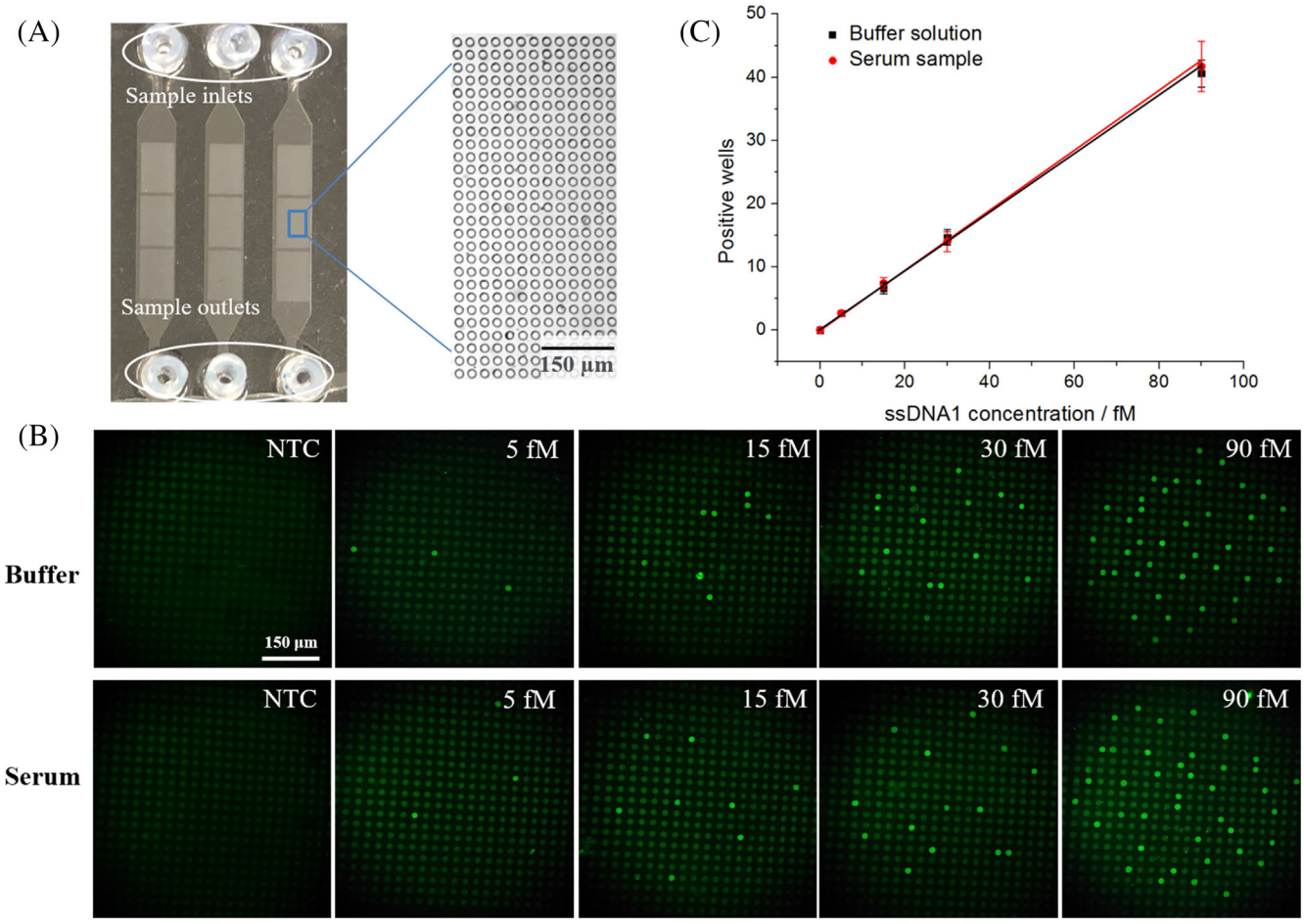

FIGURE 7 (A) Photograph of the digital microfluidic chip. Reaction mixes including Cas12a protein and DNA targets were loaded into sample inlets and subsequently distributed into each individual well. (B) Images of digital Cas12a assay on the smartphone platform: spiked buffer solution (top column) and human serum samples (bottom column). The images shown in B represent the no-target control (NTC) and four samples from 5 to 90 fM (from left to right). (C) Positive wells (green spots) are plotted against ssDNA1 concentration in the buffer solution (black) and serum sample (red). Each experimental data point was repeated in triplicate [Color figure can be viewed at wileyonlinelibrary.com]

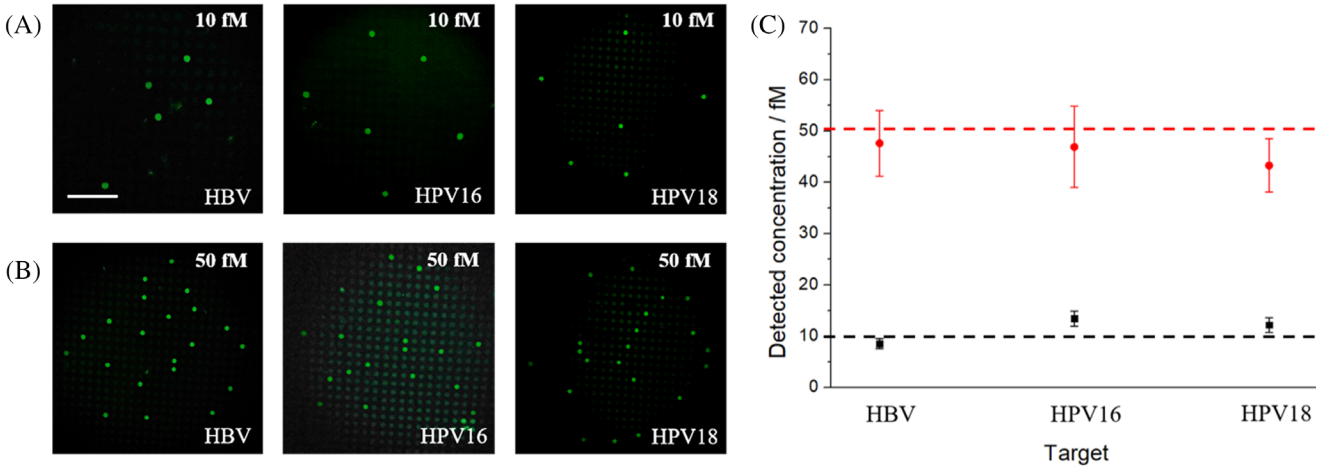

FIGURE 8 Cas12a-based digital CRISPR assay on the smartphone platform. (A,B) Smartphone fluorescence images of three different targets: HBV, HPV16, and HPV18, at 10 fM (A) and 50 fM, respectively (B). The detected values of these three targets were plotted against the spiked value (black dotted line (10 fM) and red dotted line (50 fM)). Scale bar: 150 μm [Color figure can be viewed at wileyonlinelibrary.com]

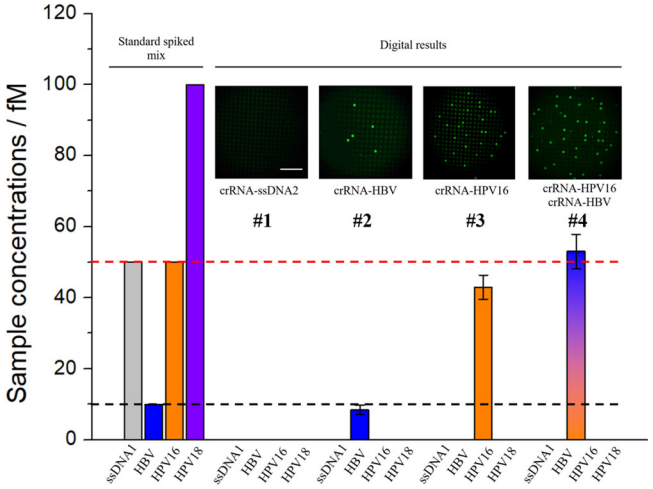

FIGURE 9 Performance of the Cas12a-based CRISPR assay for the multiplexed digital detection. The values of spiked concentrations are shown on the left (50 fM ssDNA1, 10 fM HBV, 50 fM HPV16, and 100 fM HPV 18). The fluorescence images of different chips are shown on the top, and the corresponding detected concentrations are listed below each picture. Scale bar: 150 μm [Color figure can be viewed at wileyonlinelibrary.com]

assay chip, were used in this work for running the CRISPR assay. As shown in Figure 5(A), the linear channel chip (13 × 30 × 2 mm) contained five parallel channels (width = 300 μm). Each channel contains one inlet and one outlet (I.D. = 2 mm). A smartphone fluorescent image of the chip loaded with 150 nM FAM dye is shown in **Figure S7**, indicating the uniformity of the smartphone imaging system.

The CRISPR reagents (~2 μl), including Cas12a, programed crRNA, and FQ5A reporter, were first loaded in the channels. The assay solutions were then evacuated in the vacuum to dry the reaction reagents, and the chips were stored in the refrigerator before use. The rehydrated reagents showed recovered activity of Cas12a from 40% to 60% in the next 7 days, compared with their original aqueous counterparts (**Figure S8**). Different dehydration procedures were tested, namely vacuum dry on ice, vacuum dry at 20°C, and evaporation dry at 40°C. Among the three, vacuum dry on the ice showed the best activity recovery (**Figure S8**).

In a proof-of-concept experiment, ~5 μl of analyte solutions (ssDNA1 in PBS buffer; [ssDNA1] = 0, 0.2, 1, 5 to 20 nM) were added into the inlets of the chip and quickly diffused into channels to rehydrate the CRISPR reagents. After 30 min of one-step reaction at 37°C, the microfluidic chip was inserted into the smartphone attachment for image collection. Figure 5(D) shows a typical smartphone fluorescence image of the chip, which was captured after 30 min of reaction time. Five microfluidic channels exhibited different fluorescence intensities, corresponding to different analyte concentrations. For intensity analysis, the average gray values of pixels in the yellow squares were used to quantify the fluorescence intensity from each channel (Figure 5(D)). The experiment was repeated five times independently, and the results are shown in a box chart (Figure 5(E)). The smartphone-microfluidic platform can clearly differentiate 200 pM of targets from the blank control (Figure 5(E) $p < 0.001$).

Then, multiplexed detection was performed with the linear channel chip on the smartphone platform. ssDNA targets (sDNA1, ssDNA2, ssDNA3, and ssDNA oligos that are specific to HBV) and dsDNA targets (HPV16, HPV18) were chosen to demonstrate the multiplexing ability of the smartphone–CRISPR diagnostic system (Figures 6 and S9; see sequences in Table S1). The LODs of these targets (ssDNA2, ssDNA3, HBV, HPV16, and HPV18) by the one-step Cas12a assay were all around 10 pM when measured by the plate reader (**Figure S10**). In the smartphone platform, the detection channels were pre-loaded with CRISPR reagents for ssDNA1, HBV, HPV16, HPV18, and blank control, respectively (Figure 6(A)). The analyte solutions contained different combinations of multiple DNA targets ranging from 0.2 to 10 nM (Figure 6(B–E)). As shown in Figure 6 (A), detectable fluorescent signals were generated when there was a target present in the corresponding detection channel, and the intensities were correlated with the concentration of target. The averaged green pixel (*G*) values of each channel were analyzed for the quantitative measurement of different targets (Figure 6(B–E)). A threshold line (blue dashes) at the gray value of 39 (corresponding to 0.2 nM ssDNA in Figure 5(E)) was used to exclude nonspecific autofluorescence or false positive signals from the channels. Four different mixing ratios (ssDNA1:HBV:HPV16:HPV18 = 0:0:5:0, 1:1:1:1, 0:5:0:5, and 0.2:1:10:2) were prepared to challenge the smartphone system. The platform accurately detected all samples tested, including the copresence of ssDNA and dsDNA targets (Figure 6(B–E)). Similar multiplexed detection performance was also achieved with four additional ssDNA targets (ssDNA1, ssDNA2, ssDNA3, and HBV) on the smartphone (**Figure S9**).

3.5 | Development of the digital CRISPR–Cas12a assay

In the abovementioned on-chip multiplexed detection, as low as 200 pM target DNA can be detected with the smartphone (Figure 5(D)). To further improve the detection sensitivity, we converted the bulk solution-based analog CRISPR assay into the microwell-based digital assay format with a digital microfluidic chip (Figure 7(A)). PDMS-based microarrays were prepared through a standard photolithography protocol (see Section 2). For the digital reaction, CRISPR reagents and DNA targets were first pipetted into the main channel of the digital chip at a flow rate of 100 μl/min. The concentration of Cas12a and crRNA used in the chip was 2 and 1 pM, respectively, which achieved the highest cleavage rate based on the optimization test (**Figure S11**). Then, mineral oil was injected into the chip (150 μl/min) through the main channel to seal the microwells (**Figure S12**). Finally, the digital chip was placed in the oven to start the CRISPR reaction (37°C, 90 min). We performed the digital assay for various concentrations of ssDNA1, ranging from 0 to 90 fM in buffer solution and denatured human serum samples, and the

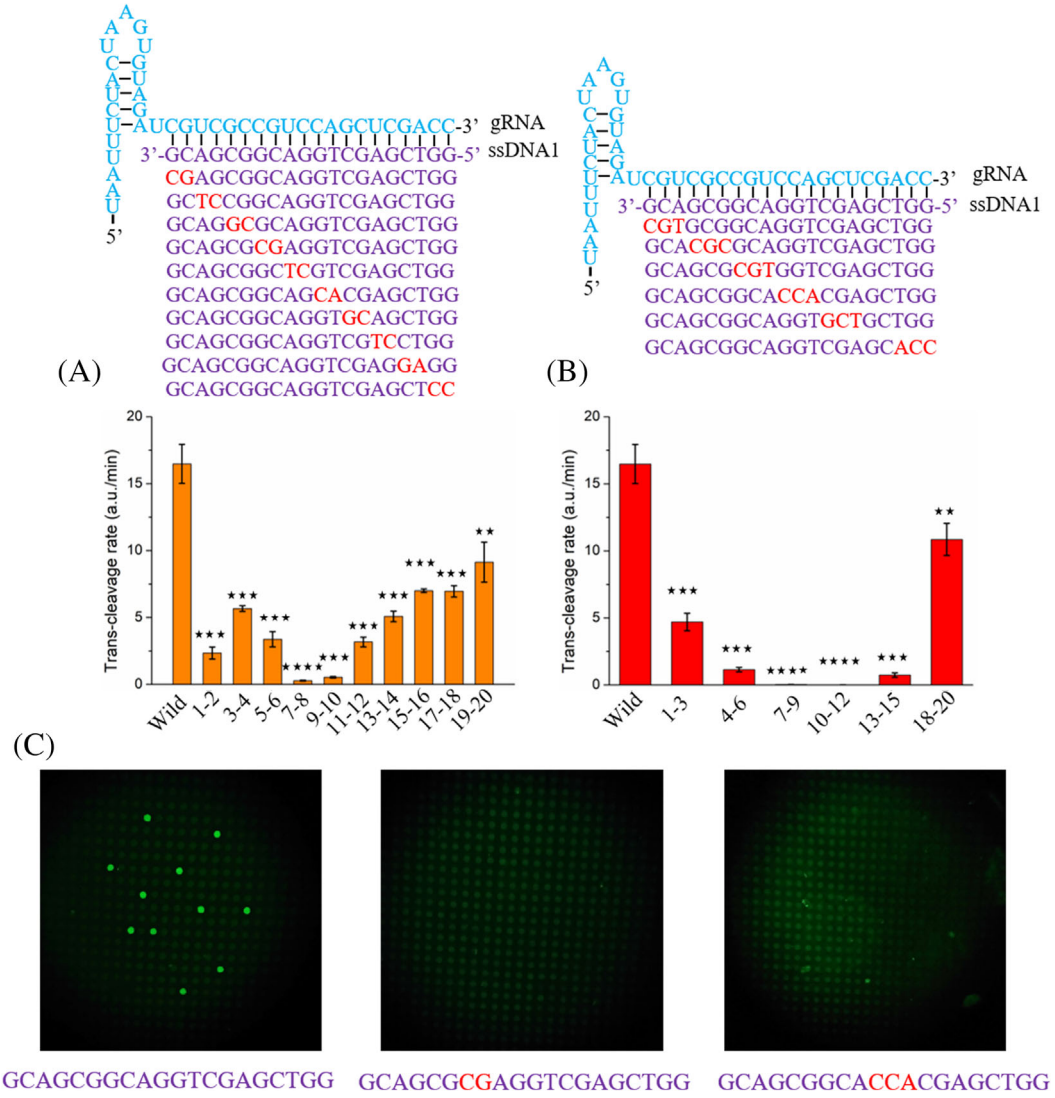

FIGURE 10 Specificity analysis of the Cas12a/gRNA detection platform. The sequences of 20-nt probe section of the gRNA and mutated ssDNA1 are listed on the top of histogram (the mismatched bases in target ssDNA are marked in red). The reaction rate of Cas12a toward double-base (A) and triple-base (B) mutations in target ssDNA1 were plotted against the mutation positions. All the data points were measured three times. The *p* values were calculated via two-sample Student's *t*-test by setting target data set as one population and the rest of the data sets as the other. **represents $p < 0.01$, ***represents $p < 0.001$, and ****represents $p < 0.0001$. (C) Fluorescence images of wild and mutated (two and three bases mutations, marked in red) ssDNAs on the digital chip, the images were captured by the smartphone device [Color figure can be viewed at wileyonlinelibrary.com]

signals were collected by both smartphone device (Figure 7(B)) and benchtop microscope (**Figure S13**). As the target concentration increased, more positive wells (green spots) were observed from the fluorescence images. Two linear calibration curves (Figure 7(C), black for buffer and red for serum sample) were obtained by plotting the number of positive wells against the concentration of ssDNA1. Both smartphone reader and conventional benchtop microscope provided comparable detection sensitivity down to 5 fM targets (Figure 7 and **Figure S13**). Compared with the previous analog CRISPR assay in the 96-well plate (Figure 3B), the sensitivity of the digital CRISPR assay was increased by ~3 orders of magnitude.

Later, we also performed the multiplexed digital assay on the smartphone platform. Six samples, including HBV, HPV16, and HPV18 targets at concentrations of 10 and 50 fM respectively, were used to test the smartphone–digital CRISPR system. Representative fluorescence images of the digital assay captured by the smartphone are shown in Figure 8(A,B). In each chip with specific crRNA, the fraction of positive fluorescence wells matched with the spiked concentration well, and the detected target concentrations agreed with the true target concentrations (Figure 8(C)). The smartphone results were also comparable with the results obtained from the benchtop microscope (**Figure S14**), indicating the reliability of the smartphone platform.

Then, a sample mixture containing 50 fM ssDNA1, 10 fM HBV, 50 fM HPV16, and 100 fM HPV 18 was used to test the multiplexed ability of the digital CRISPR chips. Four kinds of digital chips with different crRNA were used to detect corresponding target (s) in the sample

mixture: ssDNA2 chip (#1), HBV chip (#2), HPV16 chip (#3), and HPV16 and HBV chip (#4). As shown in Figure 9, no fluorescence was detected in chip #1, since there was no matched target in the sample mixture. For chips #2 and #3, the corresponding targets, HBV and HPV16, were detected, respectively. Finally, chip #4 was preloaded two different crRNA toward HBV and HPV16, and therefore generated combined fluorescent signals for HBV and HPV16 targets.

Finally, to test the specificity and effectiveness of the assay, different mismatches were introduced to the crRNA–ssDNA pairs. As a proof of concept, ssDNA1 was selected as the wild DNA, the trans-cleavage rate of the FQ5A was plotted against the different positions for the double base (Figure 10(A)) and triple base (Figure 10(B)) mutations. The mismatched bases in the target ssDNA1 were marked in red. The double-base mutations on positions 7–8 and 9–10 had the strongest deactivation effect (~95–98% reduction) of the trans-cleavage ability of Cas12a, where the other positions dropped by ~50% to ~85% of the original activity (Figure 10(A)). For triple-base mutations, the Cas12a was broadly inhibited for most mutation positions. The Cas12a showed nearly no activities for mutations on the positions 7–9 and 10–12, and ~95% activity reduction on the positions 4–6 and 13–15 (Figure 10(B)). These results show that, compared with the two ends, the central region (e.g., positions 7–12) of the crRNA–ssDNA structure has a stronger discrimination ability for two[24,26] or three base mutations, indicating the central region is critical to the binding and activation of the Cas12a. Finally, the wild ssDNA1 and its two-base and three-base mutation ssDNA1 (20 fM) were tested in the digital chip, and the images were captured by the smartphone device (Figure 10(C)). The fluorescence results of the digital assay are consistent with the previous conclusion; however, it can detect the two-base or three-base mutation at lower concentrations (fM level).

4 | CONCLUSION

We developed a convenient, sensitive, and one-step smartphone-based CRISPR diagnostic platform to detect different DNA targets (ssDNA and dsDNA) by utilizing the trans-cleavage activity of Cas12a. The influence of target structure (e.g., length, with/without PAM) and reaction protocol on the CRISPR trans-cleavage activity was systematically investigated. Under the optimal conditions, an LOD of 8 pM was achieved by the one-step Cas12a reaction without pre-amplification and a further improved detection sensitivity down to 5 fM was obtained in the digital assay format. Finally, the chip-based CRISPR assay (both linear-channel and digital format) has been coupled with a smartphone-based fluorescence reader for the multiplexed detection of HBV and HPV target DNAs. This simple, one-step CRISPR diagnostic system can in principle be expanded to RNA targets as well, by incorporating a simple reverse transcription and RNase H step.

ACKNOWLEDGMENTS

The authors gratefully acknowledge the funding support from the NCSU Chancellor's Faculty Excellence Program and NSF Career Award (Award No. 1944167).

DATA AVAILABILITY STATEMENT

The data that supports the findings of this study are available in the supplementary material of this article.

ORCID

Chase L. Beisel https://orcid.org/0000-0003-0650-9943
Qingshan Wei https://orcid.org/0000-0003-1214-010X

REFERENCES

1. Liu X, Wang F, Aizen R, Yehezkeli O, Willner I. Graphene oxide/nucleic-acid-stabilized silver nanoclusters: functional hybrid materials for optical aptamer sensing and multiplexed analysis of pathogenic DNAs. *J Am Chem Soc*. 2013;135(32):11832-11839.
2. Kannan P, Subramanian P, Maiyalagan T, Jiang Z. Cobalt oxide porous Nanocubes-based electrochemical immunobiosensing of hepatitis B virus DNA in blood serum and urine samples. *Anal Chem*. 2019;91(9):5824-5833.
3. Li X, Scida K, Crooks RM. Detection of hepatitis B virus DNA with a paper electrochemical sensor. *Anal Chem*. 2015;87(17):9009-9015.
4. Heo J, Baik TH, Kim HH, et al. Serum hepatitis B virus (HBV) DNA levels at different stages of clinical course in patients with chronic HBV infection in an endemic area. *J Korean Med Sci*. 2003;18:686-690.
5. Heermann KH, Gerlich WH, Chudy M, Schaefer S, Thomssen R. Quantitative detection of hepatitis B virus DNA in two international reference plasma preparations. *J Clin Microbiol*. 1999;37(1):68-73.
6. Qin P, Park M, Alfson KJ, et al. Rapid and fully microfluidic Ebola virus detection with CRISPR-Cas13a. *ACS Sens*. 2019;4(4):1048-1054.
7. Yuen MF, Chen DS, Dusheiko GM, et al. Hepatitis B virus infection. *Nat Rev Dis Primers*. 2018;4:18035.
8. Krupovic M, Forterre P. Single-stranded DNA viruses employ a variety of mechanisms for integration into host genomes. *Ann N Y Acad Sci*. 2015;1341(1):41-53.
9. Nuss DL. Hypovirulence: mycoviruses at the fungal-plant interface. *Nat Rev Microbiol*. 2005;3:632-642.
10. Szekely AJ, Breitbart M. Single-stranded DNA phages: from early molecular biology tools to recent revolutions in environmental microbiology. *FEMS Microbiol Lett*. 2016;363(6):fnw027.
11. Daya S, Berns KI. Gene therapy using adeno-associated virus vectors. *Clin Microbiol Rev*. 2008;21(4):583-593.
12. Wu DC, Lambowitz AM. Facile single-stranded DNA sequencing of human plasma DNA via thermostable group II intron reverse transcriptase template switching. *Sci Rep*. 2017;7(1):8421.
13. Huang X, Zhao Q, An X, et al. The ratio of ssDNA to dsDNA in circulating cell-free DNA extract is a stable indicator for diagnosis of gastric cancer. *Pathol Oncol Res*. 2020;26:2621-2632.
14. Lu S, Hu T, Wang S, Sun J, Yang X. Ultra-sensitive colorimetric assay system based on the hybridization chain reaction-triggered enzyme cascade amplification. *ACS Appl Mater Interfaces*. 2017;9(1):167-175.
15. Lu S, Wang S, Zhao JB, Sun J, Yang X. Fluorescence light-up biosensor for MicroRNA based on the distance-dependent photoinduced electron transfer. *Anal Chem*. 2017;89(16):8429-8436.
16. Lu S, Wang S, Zhao J, Sun J, Yang X. Classical triplex molecular beacons for MicroRNA-21 and vascular endothelial growth factor detection. *ACS Sens*. 2018;3(11):2438-2445.
17. Cox KJ, Subramanian HKK, Samaniego CC, Franco E, Choudhary A. A universal method for sensitive and cell-free detection of CRISPR-associated nucleases. *Chem Sci*. 2019;10:2653-2662.
18. Abudayyeh OO, Gootenberg JS, Kellner MJ, Zhang F. Nucleic acid detection of plant genes using CRISPR-Cas13. *CRISPR J*. 2019;2(3):165-171.
19. Gootenberg JS, Abudayyeh OO, Lee JW, et al. Nucleic acid detection with CRISPR-Cas13a/C2c2. *Science*. 2017;356:438-442.

20. Gootenberg JS, Abudayyeh OO, Kellner MJ, Joung J, Collins JJ, Zhang F. Multiplexed and portable nucleic acid detection platform with Cas13, Cas12a, and Csm6. *Science*. 2018;360:439-444.
21. Myhrvold C, Freije CA, Gootenberg JS, et al. Field-deployable viral diagnostics using CRISPR-Cas13. *Science*. 2018;360:444-448.
22. Bruch R, Baaske J, Chatelle C, et al. CRISPR/Cas13a-powered electrochemical microfluidic biosensor for nucleic acid amplification-free miRNA diagnostics. *Adv Mater*. 2019;31(51):1905311.
23. Li SY, Cheng QX, Wang JM, et al. CRISPR-Cas12a-assisted nucleic acid detection. *Cell Discov*. 2018;4:20.
24. Teng F, Guo L, Cui T, et al. CDetection: CRISPR-Cas12b-based DNA detection with sub-attomolar sensitivity and single-base specificity. *Genome Biol*. 2019;20:132.
25. Liang M, Li Z, Wang W, et al. A CRISPR-Cas12a-derived biosensing platform for the highly sensitive detection of diverse small molecules. *Nat Commun*. 2019;10:3672.
26. Chen JS, Ma E, Harrington LB, et al. CRISPR-Cas12a target binding unleashes indiscriminate single-stranded DNase activity. *Science*. 2018;360:436-439.
27. Huang Z, Tian D, Liu Y, et al. Ultra-sensitive and high-throughput CRISPR-p owered COVID-19 diagnosis. *Biosens Bioelectron*. 2020; 164:112316.
28. Qian C, Wang R, Wu H, Zhang F, Wu J, Wang L. Uracil-mediated new photospacer-adjacent motif of Cas12a to realize visualized DNA detection at the single-copy level free from contamination. *Anal Chem*. 2019;91(17):11362-11366.
29. Mukama O, Wu J, Li Z, et al. An ultrasensitive and specific point-of-care CRISPR/Cas12 based lateral flow biosensor for the rapid detection of nucleic acids. *Biosens Bioelectron*. 2020;159:112143.
30. Zhou R, Li Y, Dong T, Tang Y, Li F. A sequence-specific plasmonic loop-mediated isothermal amplification assay with orthogonal color readouts enabled by CRISPR Cas12a. *Chem Commun*. 2020;56:3536-3538.
31. Broughton JP, Deng X, Yu G, et al. CRISPR-Cas12-based detection of SARS-CoV-2. *Nat Biotechnol*. 2020;38:870-874.
32. Li L, Li S, Wu N, et al. HOLMESv2: a CRISPR-Cas12b-assisted platform for nucleic acid detection and DNA methylation quantitation. *ACS Synth Biol*. 2019;8:2228-2237.
33. Li Y, Mansour H, Wang T, Poojari S, Li F. Naked-eye detection of grapevine red-blotch viral infection using a plasmonic CRISPR Cas12a assay. *Anal Chem*. 2019;91(18):11510-11513.
34. Wang B, Wang R, Wang D, et al. Cas12aVDet: a CRISPR/Cas12a-based platform for rapid and visual nucleic acid detection. *Anal Chem*. 2019;91(19):12156-12161.
35. Wang Y, Ke Y, Liu W, Sun Y, Ding X. A one-pot toolbox based on Cas12a/crRNA enables rapid foodborne pathogen detection at Attomolar level. *ACS Sens*. 2020;5:1427-1435.
36. Yin K, Ding X, Li Z, Zhao H, Cooper K, Liu C. Dynamic aqueous multiphase reaction system for one-pot CRISPR-Cas12a-based ultrasensitive and quantitative molecular diagnosis. *Anal Chem*. 2020; 92:8561-8568.
37. Dai Y, Somoza RA, Wang L, et al. Exploring the trans-cleavage activity of CRISPR-Cas12a (cpf1) for the development of a universal electrochemical biosensor. *Angew Chem Int Ed Engl*. 2019;58:17399-17405.
38. Zhang D, Yan Y, Que H, et al. CRISPR/Cas12a-mediated interfacial cleaving of hairpin DNA reporter for electrochemical nucleic acid sensing. *ACS Sens*. 2020;5:557-562.
39. Nouri R, Jiang Y, Lian XL, Guan W. Sequence-specific recognition of HIV-1 DNA with solid-state CRISPR-Cas12a-assisted nanopores (SCAN). *ACS Sens*. 2020;5:1273-1280.
40. Kuhnemund M, Wei Q, Darai E, et al. Targeted DNA sequencing and in situ mutation analysis using mobile phone microscopy. *Nat Commun*. 2017;8:13913.
41. Joh DY, Hucknall AM, Wei Q, et al. Inkjet-printed point-of-care immunoassay on a nanoscale polymer brush enables subpicomolar detection of analytes in blood. *Proc Natl Acad Sci U S A*. 2017;114 (39):E7054-E7062.
42. Li Z, Paul R, Ba Tis T, et al. Non-invasive plant disease diagnostics enabled by smartphone-based fingerprinting of leaf volatiles. *Nat Plants*. 2019;5:856-866.
43. Li Z, Zhang S, Yu T, Dai Z, Wei Q. Aptamer-based fluorescent sensor array for multiplexed detection of cyanotoxins on a smartphone. *Anal Chem*. 2019;91(16):10448-10457.
44. Wu H, Qian C, Wu C, et al. End-point dual specific detection of nucleic acids using CRISPR/Cas12a based portable biosensor. *Biosens Bioelectron*. 2020;157:112153.
45. He Q, Yu D, Bao M, et al. High-throughput and all-solution phase African swine fever virus (ASFV) detection using CRISPR-Cas12a and fluorescence based point-of-care system. *Biosens Bioelectron*. 2020; 154:112068.
46. Ning B, Yu T, Zhang S, et al. A smartphone-read ultrasensitive and quantitative saliva test for COVID-19. *Sci Adv*. 2021;7(2): eabe3703.
47. Strohkendl I, Saifuddin FA, Rybarski JR, Finkelstein IJ, Russell R. Kinetic basis for DNA target specificity of CRISPR-Cas12a. *Mol Cell*. 2018;71(5):816-824.
48. Hsieh K, Zhao G, Wang TH. Applying biosensor development concepts to improve preamplification-free CRISPR/Cas12a-dx. *Analyst*. 2020;145:4880-4888.
49. Yao Q, Wang Y, Wang J, et al. An ultrasensitive diagnostic biochip based on biomimetic periodic nanostructure-assisted rolling circle amplification. *ACS Nano*. 2018;12(7):6777-6783.

SUPPORTING INFORMATION

Additional supporting information may be found online in the Supporting Information section at the end of this article.

How to cite this article: Yu T, Zhang S, Matei R, Marx W, Beisel CL, Wei Q. Coupling smartphone and CRISPR–Cas12a for digital and multiplexed nucleic acid detection. *AIChE J*. 2021;e17365. https://doi.org/10.1002/aic.17365